Gold-nickel nanowires as nanomotors for cancer marker biodetection and chemotherapeutic drug delivery

Gold-Nickel Nanowires as Nanomotors for Cancer Marker Biodetection and Chemotherapeutic Drug Delivery

Gozde Yurdabak Karaca, Filiz Kuralay,[*] Emre Uygun, Kadir Ozaltin, Sezin Eren Demirbuken, Bora Garipcan, Lutfi Oksuz, and Aysegul Uygun Oksuz[*]

Gozde Yurdabak Karaca − Department of Bioengineering, Suleyman Demirel University, Isparta 32260, Turkey; Department of Chemistry, Suleyman Demirel University, Isparta 32260, Turkey; orcid.org/0000-0002-5371-2613

Emre Uygun − Department of Civil Engineering, Suleyman Demirel University, Isparta 32260, Turkey; orcid.org/0000-0003-3792-1922

Kadir Ozaltin − Centre of Polymer Systems, Tomas Bata University in Zlin, Zlin 76001, Czech Republic; orcid.org/0000-0002-7619-5321

Sezin Eren Demirbuken − Institute of Biomedical Engineering, Bogazici University, Istanbul 32260, Turkey; orcid.org/0000-0001-9393-0677

Bora Garipcan − Institute of Biomedical Engineering, Bogazici University, Istanbul 32260, Turkey; orcid.org/0000-0002-1773-5607

Lutfi Oksuz − Department of Physics, Suleyman Demirel University, Isparta 32260, Turkey; orcid.org/0000-0002-6207-7308

Corresponding authors

Aysegul Uygun Oksuz − Department of Chemistry, Suleyman Demirel University, Isparta 32260, Turkey; orcid.org/ 0000-0002-9487-7350; Email: ayseguluygun@sdu.edu.tr

Filiz Kuralay − Department of Chemistry, Hacettepe University, Ankara 06800, Turkey; rcid.org/0000-0003-0356-9692; Email: filizkur@hacettepe.edu.tr

ABSTRACT

Future biomedical applications of nanomachines require elimination of fuel requirements since most of the fuels have potential toxic effects. Herein, we report fuel-free magnetically powered gold-nickel (Au-Ni) nanowires as nanomotors for multipurpose biomedical applications. Fabrication of the nanowire-based nanomotors developed in this study is unique, and this protocol was dependent on the electrochemical preparation of Au nanowires followed by the direct current (DC) magnetron sputtering of Ni part. DC magnetron sputtering-based preparation used for the first time in the literature not only ensured homogeneous distribution and rapid deposition of the metal directly but also provided reproducible thin layers of magnetic Ni resulting in a significant improvement at nanomotor speeds. Besides magnetic propulsion, acoustic propulsion was also successfully applied. The effects of both propusion mechanisms were tested on the speed and direction of Au-Ni nanomotors. Biomedical applications of the motors accomplished in this study are rapid and sensitive detection of an important cancer biomarker microRNA-21 (miRNA-21) and pH-dependent and near-infrared (NIR) triggered release of a commonly used chemotherapeutic drug doxorubicin (DOX). Sensitive and selective miRNA-21 detection was achieved by using dye-labeled single-stranded DNA

(ssDNA probe) modified Au-Ni nanomotors with a wide linear concentration range of 0.01 nM to 25 nM. Low detection limits of 2.9 pM and 1.6 pM were obtained for fluorescence and speed-based detection, respectively (n = 3). In addition, magnetically powered DOX-loaded Au-Ni nanomotors were guided on cancer cells (human breast cancer cell lines, MCF-7) in a controllable way for the efficient and controlled delivery of DOX. Cytotoxicity studies of the nanomotors presented negligible influence on the cell viability.

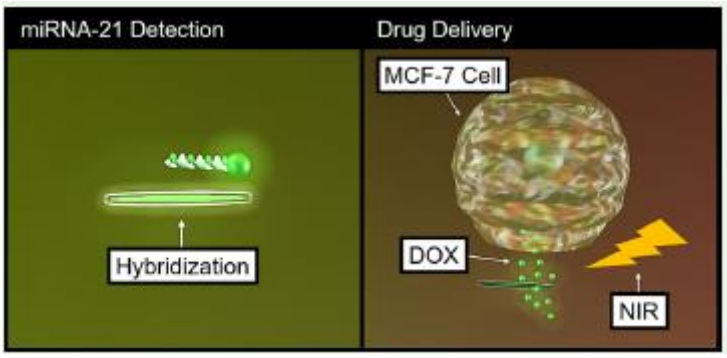

KEYWORDS: Nanowires as nanomotors, magnetic propulsion, microRNA-21, doxorubicin, cancer cell

1. INTRODUCTION

Nanotechnology has led to the development of powerful synthetic micro/nanomotors that convert energy into movement and are able to perform advanced tasks at the micro- and nanoscales.[1,2] These small motors are highly favorable for specific applications such as (bio)chemical sensing, targeted drug delivery, noninvasive surgery, security and defense, environmental monitoring and remediation, cell manipulation, and isolation.[3-5] Nanomotors can be self-propelled or externally powered in the liquid phase by different types of energy sources such as catalytic, magnetic, ultrasonic, electrical field, and light propulsion mechanisms.[6,7] These propulsion mechanisms directly affect the possible use of these motors for real-life applications. In this context, nanomotors driven by magnetic field have attracted great attention due to their certain advantages on motion control, targeted delivery, longlifetime, and have great potential for in vivo studies.[4,6] There have been important improvements with the advances of these propulsion mechanisms in the micro/nanomotor field. For example, Li et al. have investigated a magneto-acoustic hybrid fuel-free nanomotor which could be controlled by both ultrasound and magnetic field.[8] They have used these external fields according to their biocompatible energy and extensive use in monitoring, diagnostic, and drug delivery applications. For controlled cargo release in biological fluids, Liu et al. have described magnetically actuated nanomotors based on 6-carboxyfluorescein (FAM) release from functionalized magnetic nanomotors.[9] Cai et. al have presented the advantages of zinc oxide (ZnO) and nickel (Ni) to fabricate ZnO-Ni microrockets that provided effective magnetic control.[10]

Owing to micro and nanomotors' inimitable properties, including autonomous motion, easy surface functionalization, availability for effective capture, and isolation of target analytes, they look promising for various biomedical applications such as diagnosis of diseases.[11] As an example, de Avila et al. have described a fluorescence strategy for detecting the endogenous content of microRNA-21 (miRNA-21) based on an ultrasound propelled gold (Au) nanomotor functionalized with singlestranded DNA (ssDNA).[12] Nelson et al. have demonstrated a magnetic microswimmer functionalized with plasmid

DNA (pDNA) for biosensing and targeting cancer cells.[13] In addition, Wang et al. have used gold nanowires that were functionalized with enzyme for targeting cancer cells.[14] Graphene-oxide coated gold nanowire motors functionalized with fluorescein-labeled DNA aptamers for qualitative detection of overexpressed AIB1 oncoproteins in MCF-7 breast cancer cells have been studied by Beltran-Gastelum.[15]

When it comes to drug delivery, Wang's group has established the first proof of concept of chemically powered catalytic micromotors as liposomal and polymeric drug carriers.[16] Sanchez et al. have demonstrated urease powered nanomotors for anticancer drug doxorubicin (DOX) loading and release to cancer cells.[17] Garcia-Gradilla et al. have stated that the ultrasound propelled nanowire motors with improved drug loading capacity provided a good approach for the rapid and efficient delivery of therapeutic payloads.[18] Magnetically driven thumbtack-like and frisbee-like chitosan and calcium alginate hydrogel DOX-loaded microrobots have been fabricated for pH-sensitive drug release by Xie et al.[19] Another study showing the significant potential of nanomotors for biomedical applications has been performed by He et al.[20] They have exploited DOX encapsulated motors navigated to cancer cells by magnetic field for drug delivery and release under NIR light.[20] Singh et al. have demonstrated molybdenum disulfide-based tubular microengines used for efficient drug loading (DOX) and release. In addition, they have presented the use of fluorescent detection of miRNA-21.[21] The noteworthy capabilities of fuel-free acoustically driven functionalized Au-Ni-Au nanowires have been reported by Garcia-Gradilla et al. for pH-sensitive drug loading with the use of polystyrene sulfonate (PSS) layer.[22] Jiao et al. have developed a Au sputtered Janus mesoporous nanocarrier with NIR propulsion for cell interaction.[23]

In the light of these published works, we aimed to develop novel and different nanomaterials that were propelled under controllable magnetic field since magnetic propulsion could be more convenient for most of the real-life applications such as biosensing and disesase therapy. These nanomaterials based on Au-Ni nanowires as nanomotors were constructed by the electrochemical preparation of the Au segment using conventional template-assisted deposition steps be pursued by the direct current (DC) magnetron sputtering of the Ni segment onto Au nanowires. Conventional methods for the formation of magnetic Ni segments commonly include template-assisted electrochemical deposition of the metal.[24,25] In addition, there have been several works apart from electrochemical deposi-tion.[23] Directional control of micromotors under an external magnetic field has been achieved by Cai et al. using titanium dioxide-iron (TiO_2-Fe) Janus micromotors with sputtered magnetic layer.[26] A bubble-propelled catalytic Janus micromotor has been demonstrated by Wu and his group.[27] This motor has been based on a porous polystyrene (PS) sphere which was half-coated with Ni-Fe by a magnetron sputtering method to accomplish magnetic guidance. In this study, the magnetic segment of the motors were created by DC magnetron sputtering. This fabrication resulted in several superior characteristics such as homogeneous distribution of Ni metal onto Au nanowire structures, rapid and reproducible formation of the magnetic segment, and magnetic motors with higher speeds compared to the other magnetically propelled nanomotors. Furthermore, metal deposition from the Ni target served direct preparation and prevented any other chemical reagent utilization. Then the biomedical applications of these nanowires as nanomotors were performed for an important cancer biomarker miRNA-21 which was used mainly for the diagnosis of solid tumors including mainly breast, colorecteral, prostate, gastric, pancreatic, and lung cancers[28,29] and controlled and triggered the release of a commonly used antitumor agent Doxorubicin.[30,31] For the biosensing study, the proposed nanomotors provided highly sensitive, selective, and reproducible results for miRNA-21 detection. For the drug delivery approach, improvement in the nanomotor speeds provided controllable changes under implemented factors including NIR triggered and pH-dependent studies. Quartz crystal microbalance (QCM) spectroscopy and ultraviolet-visible (UV-vis) spectroscopy were also used to

follow up on the released drug, and all the results were well correlated. In vitro applications of the Au-Ni nanowires as nanomotors were successfully accomplished. Cytotoxicity tests were performed and 24 h toxicity studies showed that the nanomotors had insignificant influence on the cell viability. Thus, these novel magnetic nanomotors offer considerable potential for the construction of rapid and reliable cancer detection and efficient drug delivery systems with their reproducible, practical, and low-cost fabrication, effective surface, motion controllability, and targeted transport.

2. MATERIALS AND METHODS

2.1. Reagents and Solutions

Bovine serum albumin (BSA), ethylenediamine tetraacetic acid (EDTA), Tris-HCl, and doxorubicin hydrochloride were purchased from Sigma-Aldrich. Oligonucleotides were purchased from Heliks Biotechnology (Turkey). The oligonucleotides used in the study are listed below:

6-carboxyfluorescein dye-labeled-single-stranded DNA probe (FAM-ssDNA anti-miRNA-21 probe): FAM-5 '-TCAACATCAGTC-TGATAAGCTA-3'

Target miRNA 21:5' -UAGCUUAUCAGACUGAUGUUGA-3'

1-Base mismatch sequence (1-MM): 5'-UAGCUUAUAAGACUG-AUGUUGA-3'

2.1.1. Preparation of Solutions

Oligonucleotide solutions were dissolved in pH 8.0 10 mM Tris-EDTA (TE) buffer prepared innuclease-free water (containing 1 mM EDTA) and separated into small 100 pM aliquots. The solutions were stored at -20 °C until use. For FAM-labeled ssDNA probe immobilization, 20 mM Tris-HCl containing 100 mM NaCl and 5 mM MgCl2 were prepared with Milli-Q water. Twenty mM pH 7.4 Tris-HCl containing 100 mM NaCl and 1 mM EDTA was used for the hybridization studies. Washing steps were performed with 100 pg mL^{-1} of bovine serum albumin (BSA).

2.2. Instrumentation

Template electrochemical deposition of nanowires was carried out with a CHI 720E potentiostat (CH Instruments, CHI). A Nikon Instrument Inc. Ti Optic LV100ND Model optical microscope was used for measuring and displaying the fluorescence intensity and speed of nanomotors. The motion videos of nanomotors were taken at 100X magnification at a frame rate of 5 s^{-1}. According to the literature, the emission wavelength of DOX covers both green and red light, with green light being predominant. Also, the green fluorescence imaging intensity of DOX has a higher sensitivity than the red fluorescence.[32] DAPI (4',6-diamidino-2-phenylindole) filter (green filter, excitation at 470 nm) was used for fluorescence measurements. Due to the specifications of this microscope set up DOX/PSS/Au-Ni nanomotors showed green fluorescence in parallel to literature.[18]

To magnetically operate the Au-Ni nanowire as a nanomotor, an external magnetic field, 22 mT, was applied by placing a coil 6 cm away from the glass slide without changing the distances. Movement studies at different frequencies were performed using an alternating magnetic field (0-20 Hz) at a specific speed. The manipulations of the magnetic nanomotors and their motion were tracked using the optical microscope. For acoustic propulsion of the nanomotors, a surface acoustic wave (SAW) system was used.[33] The solution in the cell was excited by a piezoelectric electrode which includes a 128° rotated Y cut-X propagation lithium niobate ($LiNbO_3$) substrate with interdigital transducers (IDTs)

deposited on it and a square glass capillary. The resonant frequency of the cell center was (96 ± 0.01) MHz, and the standing surface acoustic wave wavelength was 40 μm. The power, a peak to peak value of 5 dBm, was applied using a waveform generator. The combined effect of the magnetic-acoustic power on the propulsion performance of the Au-Ni nanomotors was investigated under different operation modes using this setup. Precise control of the magnetic propulsion of the Au-Ni nanomotors were achieved using an external magnet next to a SAW cell that created a uniform 22 mT magnetic field described above. The behavior of the magnetically propelled nanomotors in the presence of an acoustic field was analyzed and compared with their behavior in the absence of an acoustic field.

The structural morphology and elemental analysis of the Au-Ni nanomotor were examined using scanning electron microscopy-energy dispersive X-ray spectroscopy (SEM-EDS), FEI Quanta FEG 250 Model. UV-vis spectroscopy analysis was performed using a PerkinElmer UV/vis spectrometer, Lambda 20. Maxtek Inficon RQCM (RQCM Maxtek, U.S.A.) 5 MHz AT-cut quartz crystal device was used by conjunction with a computer program to monitor real-time resonance frequency change. A gold-plated 5-MHz AT-cut quartz crystal and a flow cell (Inficon Maxtek, FC-550) were used in drug loading and release applications. The drug solution was pumped (Instech, model P720 peristaltic pump) continuously into a closed loop through the flow cell by optimizing at a flow rate of 10 μL min^{-1}.

2.3. Synthesis of Au-Ni Magnetic Nanowires. The gold

The gold nanowires were fabricated using a common template-electrodeposition technique. A silver film was sputtered (RF magnetron sputtering, 40 W, 15 mTorr) on one side of the porous alumina membrane (AAO) template containing 0.2 µm diameter pores (Catalog No 6809-6022; Whatman, U.K.) to use as a working electrode. The membrane was assembled in a plating cell with aluminum foil serving as the contact for the sputtered silver side. Platinum counter electrode and Ag/AgCl reference electrode were purchased from CHI and utilized. The Au wire was electrodeposited in the branch area of the membrane from the commercial gold plating solution (Orotemp 24 RTU RACK; Technic, Inc., Anaheim, CA, U.S.A.) at -0.05A during 3600 s. The sputtered silver layer was mechanically removed from the membrane by hand polishing it with a 3-4 μm alumina slurry. Then the membrane was dissolved in 4 M NaOH solution for 20 min to completely release the gold nanowires. The nanowires were collected by centrifugation at 6000 rpm for 5 min and washed repeatedly with deionized water (18.2 MΩ cm at room temperature), three times each, with centrifugation for 5 min following each wash. After the nanowires in pure water were centrifuged, the water was carefully removed and ethanol (99.8%) was added. The dispersed nanowires in ethanol were dipped onto a clean slide and dried. The Au nanowires coated on the glass substrate were placed in a DC magnetron sputter system for Ni coating. The DC magnetron sputter system pressure dropped to 50 mTorr, under argon gas flow. Ni coating was realized under 150 mTorr pressure and 300 W power for 15 min.

2.4. ssDNA Probe Immobilization onto Au-Ni Nanowires and Target miRNA-21 Detection

Au-Ni nanomotors were incubated with 60 μM FAM-labeled ssDNA probe solution for 30 min at room temperature. FAM-ssDNA has bound nonspecifically to Au-Ni nanomotor surfaces, presumably by means of interactions provided through the exposed bases and the hydrophobic interaction via van der Waals forces between the nucleobases.[34] Probe immobilized Au-Ni (ssDNA/Au-Ni) nanomotors were washed with 50 μL BSA solution. Target miRNA-21 (100 nM, prepared in 20 mM pH 7.4 Tris-HCl buffer) was added to ssDNA/Au-Ni medium and incubated for different times, such as 5, 10, 15, 30, and 60 min, to perform optimization experiments. For miRNA-21 detection studies, ssDNA/Au-Ni

nanomotors were incubated with various concentrations of miRNA-21. Nanomotors were washed with BSA solution after hybridization. The same procedure was applied for the 1-M sequence to test the specificity. The biodetection strategy based on the fluorescence intensities and speed changes of the nanomotors was followed with optical microscopy.

2.5. Chemotherapeutic Drug Loading onto Au-Ni Nanomotors

The surfaces of Au-Ni nanowires as nanomotors were activated by immersing a batch of the nanomotors into 1 mL of poly(sodium 4-styrenesulfonate) (PSS) solution (2 mg mL^{-1} prepared in 6 mM NaCl) for 3 h. After incubation, the nanomotors were washed with pure water 3 times. The chemotherapeutic drug solutions (200, 100, 50, 25 μM) which were prepared in pH 8.0 phosphate buffer were loaded onto the PSS/Au-Ni nanomotors and stored at 4 °C for 24 h. After centrifugation and three cycles of washing with pH 8.0 phosphate buffer, DOX/PSS/Au-Ni nanomotors were subjected to fluorescence intensity and speed measurements using optical microscopy. Drug release was performed by changing the pH of the buffer solution from 8.0 to 5.0.

2.6. Cell Viability Experiments

Cytotoxicity testing was performed using a mouse embryonic fibroblast continuous cell line (NIH/3T3, ATCC CRL-1658TM, U.S.A.), according to the EN ISO 10993-5 standard with modification. The ATCC-formulated Dulbecco's Modified Eagle's Medium (BioSera, France), containing 10% calf serum (BioSera, France) and Penicillin/Streptomycin at 100 U mL^{-1} (PAA Laboratories GmbH, Austria) was used as a culture medium. The tested samples were diluted in the culture medium with concentrations of 5, 10, and 20% (v/v). Cells were precultivated for 24 h in a 96 well-plate, and after the cultivation process, the culture medium was subsequently replaced with diluted samples and incubated for 24 h. As a reference, cells were cultivated in a pure medium and considered as 100% viable. The changes in cell morphology were observed with an inverted fluorescent microscope (Olympus, IX 81). In order to assess the cytotoxic effect, 3-(4,5-dimethylthiazol-2-yl)-2,5-diphenyltetrazolium bromide (MTT) assay (Duchefa, Biochemie, Netherlands) was performed. The absorbance was measured by an Infinite M200 Pro NanoQuant absorbance reader (Tecan, Switzerland). All tests were performed in quadruplicate.

2.7. Zeta Potential Measurements

Au-Ni, PSS/Au-Ni and DOX/PSS/Au-Ni nanomotors were dispersed in 2 mL of pure water. Zeta potential experiments were made to determine the electrophoretic mobility using a Hariba Scientific Nanoparticle-Nanoparticle analyzer SZ-100 V2. Experiments were carried out at room temperature and measured at least three times.

2.9. In Vitro Experiments

An MCF-7 human adenocarcinoma breast cancer cell line was used in the targeted drug transport and intracellular drug release experiments. Cells were cultured in DMEM-F 12 (Dulbecco's Modified Eagle Medium-F12) supplemented with 10% FBS (Fetal bovine serum) and 1% penicillin/streptomycin (Gibco) at 37 °C in a humidified incubator with CO_2 (5%) in a T25 flask.[35] When the cells reached 80% confluence, the cells were removed with the help of 0.25% trypsin/EDTA (Gibco) to seed onto sterilized

coverslips which were accordingly placed in a 6-well plate to observe the interaction between cells and nanomotors under optical microscopy. All studies were carried out with sterilized materials in biocabins.

2.10. NIR Irradiation Triggered Intracellular Drug Release Studies

DOX release from DOX/PSS/Au-Ni nanomotors was carried out at room temperature by irradiation of the motors using near-infrared laser (at 800 nm and 20 mW). MCF-7 cells were coincubated with DOX/PSS/Au-Ni nanomotors (20 μL) in pH 8.0 phosphate buffer. The autonomous nanomotors were guided toward the MCF-7 cells by the external magnetic field (22 mT). NIR was facilitated to trigger DOX release using different durations. The fluorescence intensities of the nanomotors were monitored and analyzed by optical microscopy.

A summary of the experimental protocol including the synthesis and application of the nanomotors is given in **Scheme 1**.

Scheme 1. Summary of the Experimental Protocol

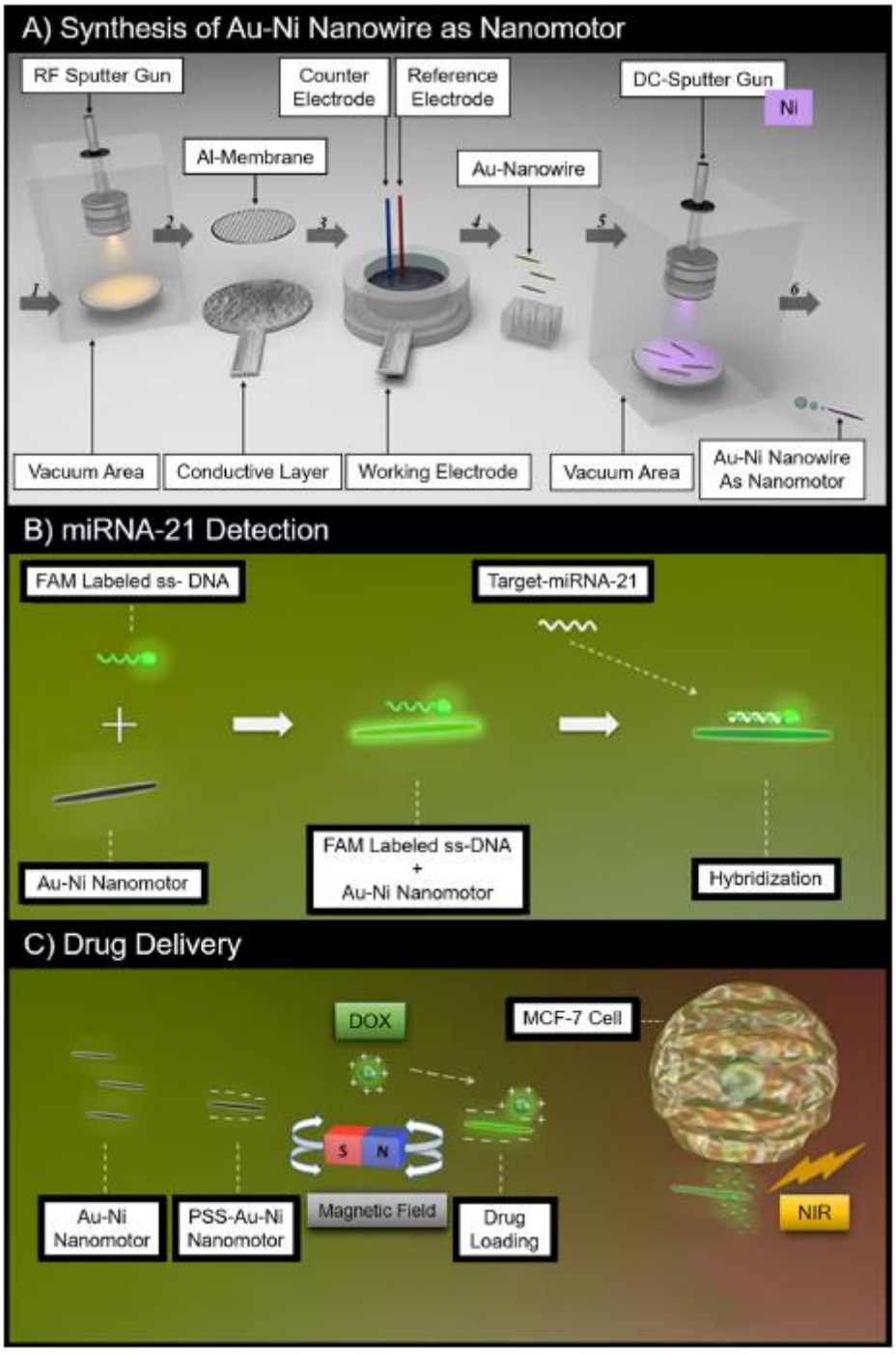

3. RESULTS AND DISCUSSION

3.1. Characterization Studies and Optimization of Magnetic

Propulsion Conditions of the Au-Ni Nanomotors. SEM characterization was performed to identify different segments of Au-Ni nanowires as nanomotors. **Figure 1**A-a shows the SEM image of a Au nanowire with 3 μm length and 200 nm diameter. The solid smooth surface of the nanowire indicates

the morphology of the gold.[12] The presence of a Ni layer onto the Au nanowires is shown in **Figure 1**A-b. The energy-dispersive X-ray (EDX) mapping analyses depicted in **Figure 1**A-c clearly revealed the presence of Au and Ni within the smooth wire shape. The separate EDX spectra of Au and Ni are given in **Figure 1**A-d and A-e. Further characterization and optimization studies were then carried out under a magnetic setup combined with the optical microscope. Schematic presentation of this setup is given in **Figure 1**B.

The traveling ability of nanomotors on a predetermined path is an important aspect of the integration of nanomotors into microfluidic networks.36 Directed motion of fuel-free Au-Ni nanowires within the microchannel network is illustrated in **Supporting Information**, **SI**, **Video S1**. Au-Ni nanowire was directed in a pattern along a 200 μm long and 77.75 μm width microchannel over 20 s. A 22 mT constant magnetic field was applied at a distance of 20 mm to observe movement of the nanowires in the microchannel. The speed of Au-Ni nanomotor was measured as 15 μm/s under 22 mT magnetic field. These magnetic nanowires appeared routable and predictable in the linear regime.[25]

In this study, the nanowire speeds were controlled by varying the frequency of the applied field. **Figure 2**A presents the dependence of the velocity on the magnetic field over the range of 0-20 Hz. The speed of the magnetic nanowire increased from 6.35 to 21.5 µm/s upon raising the frequency from 4 to 20 Hz. Gao et al. have found that flexible magnetic nanowire motor speeds increased (1.5 to 6 μm/s) with increasing magnetic field frequency (5 to 15 Hz).[25]

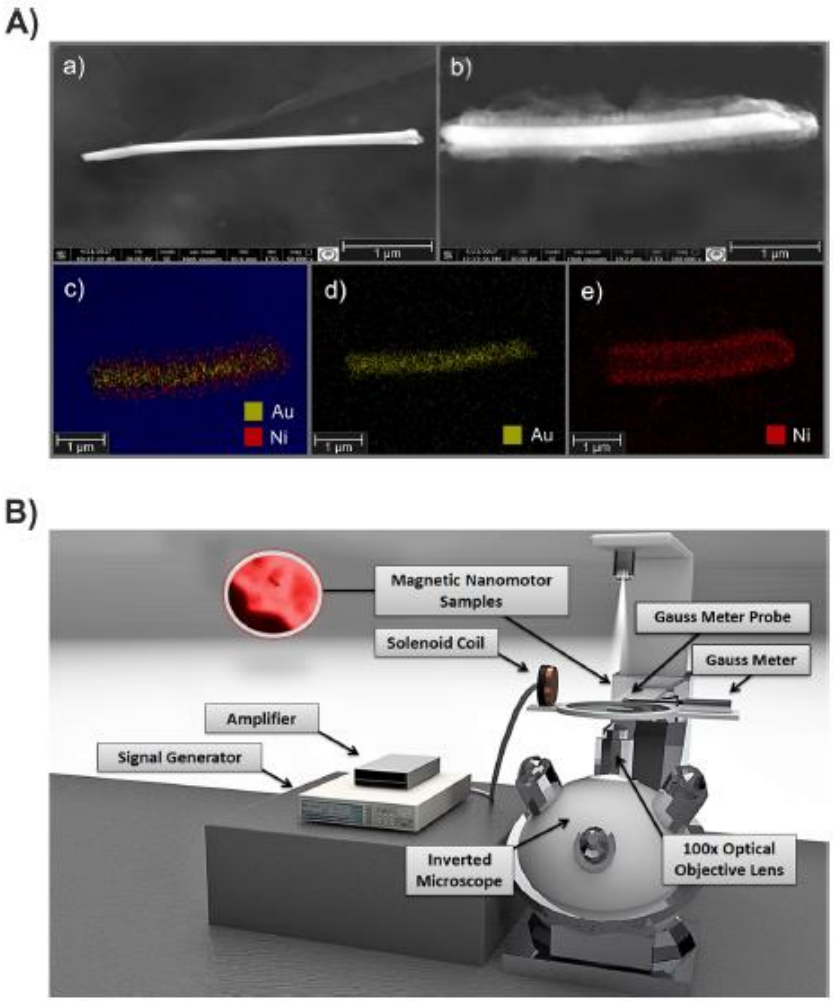

Figure 1. (A) SEM images of (a) Au nanowire, (b) Au-Ni nanowire and corresponding EDX mapping images of (c) Au-Ni nanomotor, (d) Au layer, (e) Ni laer. (B) Schematic diagram of the experimental setup.

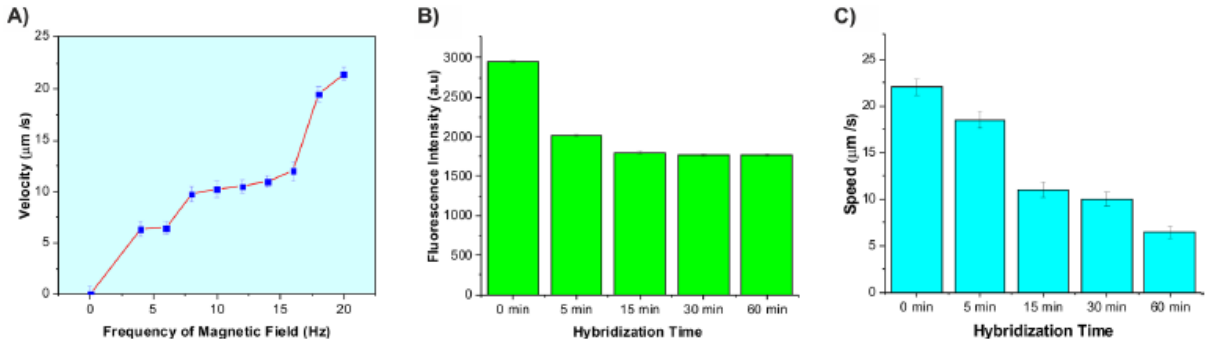

Figure 2. (A) Dependence of the speed of magnetic nanowires upon the frequency of magnetic field (0-20 Hz). Effect of hybridization time on (B) nanomotor fluorescence intensities, and (C) nanomotor velocities (**n** = 3).

In our study, Au-Ni magnetic nanowires indicated higher speed performance as 11 μm/s at 14 Hz magnetic field frequency. It can be concluded that the fabrication protocol of the magnetic segment using DC magnetron sputtering improved the velocity of the nanowire significantly.

Combining different fuel-free propulsion mechanisms into a single nanomotor such as magnetic and acoustic propulsion is quite a challenging task.[8] Herein, our Au-Ni nanomotors presented controlled motion under a magnetic and acoustic field. In addition to magnetic guidance, the acoustic field was also applied to the Au-Ni nanomotors. **Video S2** shows nanomotor behaviors under 22 mT magnetic field and both magnetic and acoustic field (3 dBm). While the speed of nanomotor measured using the magnetic mode was 20 μm/s, 120 μm/s was achieved under both magnetic and acoustic mode conditions. These nanomotors were also reoriented in a different direction and they were faster in the presence of an acoustic wave.[37] Thus, the fabricated nanomotors had the advantage of dual propulsion mechanisms which were safe and convenient technologies.

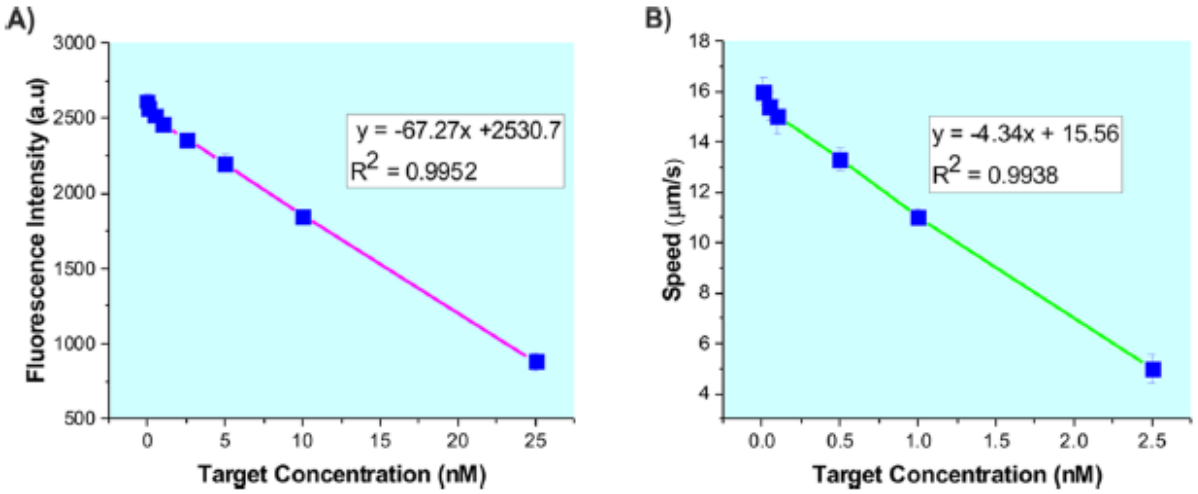

Figure 3. Calibration curves based on: (A) fluorescence intensity and (B) speed (**n** = 3).

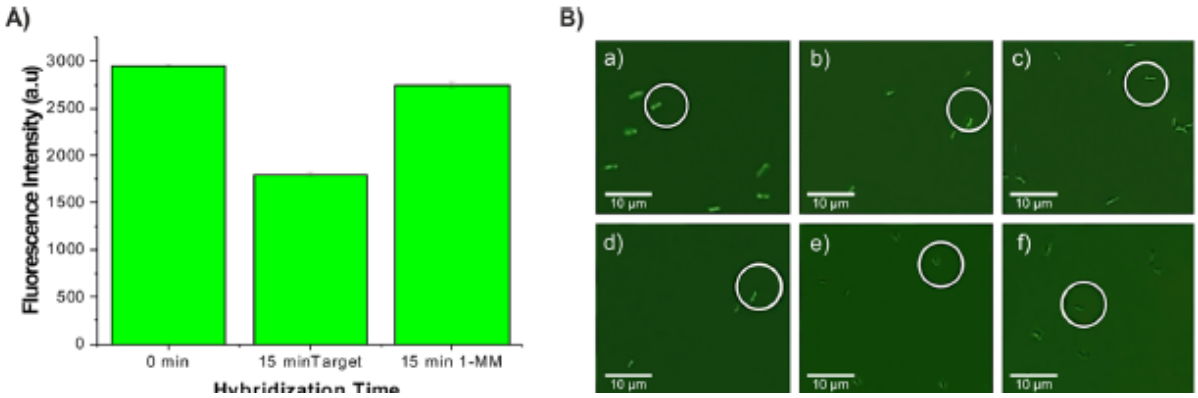

Figure 4. (A) Histogram presenting the effect of fluorescence intensity on selectivity of nanomotors (**n** = 3), (B) optical microscopy images of (a) Au-Ni nanomotors, (b) FAM-ssDNA/Au-Ni nanomotors and FAM-ssDNA/Au-Ni nanomotors incubated with (c) 0.05 nM target, (d) 0.1 nM target, (e) 50 nM target, and (f) 100 nM target.

3.2. Biosensing Applications of Au-Ni Nanowires

The miRNA-21 sensing properties of magnetic Au-Ni nanowires as nanomotors were examined based on the fluorescence quenching and the decrease in nanomotor speeds as a result of miRNA-21 recognition by the nanomotors. For this recognition, first a fluorescent dye-labeled ssDNA probe was immobilized on Au-Ni nanomotors (ssDNA/Au-Ni nanomotors). Without probe immobilization, the fluorescence intensity of the Au-Ni nanomotor was measured as 740 au After FAM-labeled ssDNA incubation, the fluorescence intensity of the nanomotor was determined as 2950 au due to FAM labeling. In the presence of the ssDNA probe, Au-Ni nanomotors hybridized with the miRNA-21 target sequence in an efficient and sensitive way. The selectivity experiment of the ssDNA/Au-Ni nanomotors was performed in the existence of 1-MM sequence and resulted in high selectivity. The fluorescence intensities and the velocities of ssDNA/Au-Ni nanomotors were changed after the hybridization with the miRNA-21 target sequence. Decreases in the intensities and speeds were obtained. Thus, a two-way detection strategy was successfully developed in the study. Detection of this hybridization could be one of the possible identifiers of specific miRNA-21 levels within cells or in tissue for important biomedical applications.[38]

In the beginning of miRNA-21 sensing studies, immobilization of the ssDNA probe was accomplished on Au-Ni nanowires by the incubation of FAM-labeled ssDNA for 30 min at room temperature. After this incubation step, ssDNA/ Au-Ni nanomotors interacted with 1 nM target miRNA-21 at various times (5 to 60 min) to determine the optimum hybridization time. These optimization studies were conducted using the changes in both the fluorescence intensity (**Figure 2**B) and the nanomotor speed (**Figure 2**C). With increasing hybridization time (from 5 to 60 min), the fluorescence intensity of the ssDNA/Au-Ni nanomotor decreased from 2016 au to 1400 au and the speed of ssDNA/Au-Ni nanomotor decreased from 18 to 7 μm/s (**Figure 2**C). It should also be noted that after 5 min of target interaction, there were still reductions in the measured values compared to the 0 min values. Quenching in the fluorescence intensity could be attributed to the internal hybrid formation on the nanomotors, while the decrease in the speed could occur due to blocking of the nanomotor surfaces as a result of this hybrid formation.[39] After 15 min of hybridization, there was no significant change in the fluorescence intensity. In addition, for the speed changes, the responses with 15 and 30 min of

hybridization times were almost the same. Thus, 15 min of hybridization time was used for the miRNA-21 detection.

Under optimal conditions, the relationships between the fluorescence intensity of the nanomotors and the concentration of the target miRNA-21 and also the speed of the nanomotors and the concentration of the target miRNA-21 were probed. With increasing target concentration from 0.01 nM to 25 nM target, the fluorescence intensities of nanomotors decreased gradually (**Figure 3**A). The decreases in the speed of nanomotors were given in **Figure 3**B. The linear miRNA-21 concentration range was between 0.01 nM to 2.5 nM for this sensing strategy.

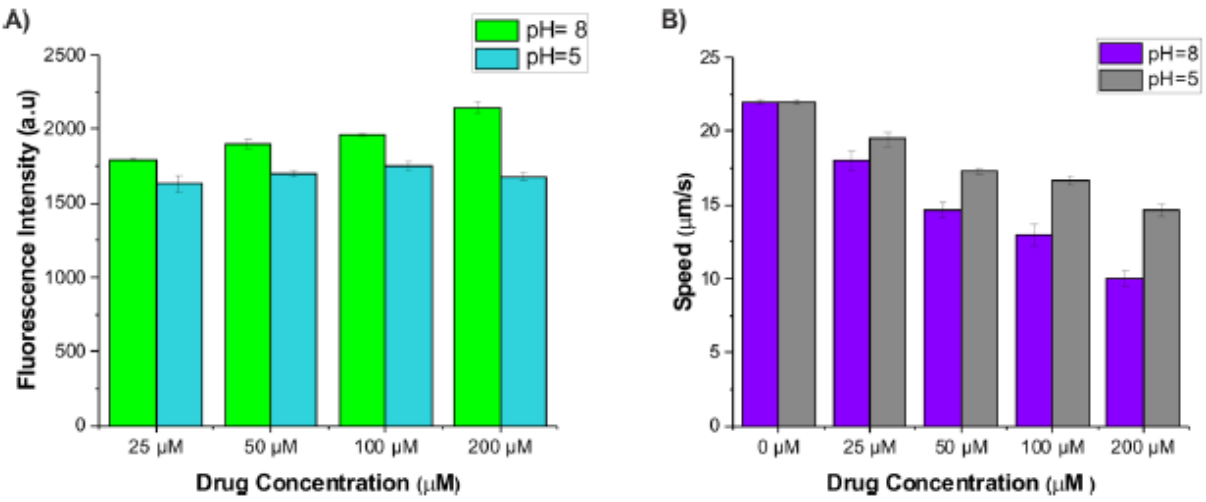

Figure 5. Effect of different concentrations of DOX on the (A) fluorescence intensity and (B) speed of PSS/Au-Ni nanomotors before and after drug unloading (n = 3).

After the 2.5 nM concentration, the movement of the Au-Ni nanomotor was not observed because of the large amount of loading onto Au-Ni nanomotors. The bar graphs for these detection studies are presented in **Figure S1-A,B**. The responses of the higher concentrations which showed the saturation levels for target miRNA-21 (50 nM and 100 nM) are included in **Figure S1-A**. After these promising responses, the limit of detection (LOD) was calculated as 2.9 pM (3 o,b/slope, where o,b was the standard deviation of blank samples) based on the declines in fluorescence intensities. It was calculated as 1.6 pM for the speed-based miRNA-21 detection strategy (n = 3). Our detection limits were lower than previous reports which studied nano/micromotors. The comparison of the results with the previous works were shown Table S1. This table emphasized and highlighted the applicability and efficiency of this new ssDNA/Au-Ni motors.

In order to present the selectivity of ssDNA/Au-Ni nanomotors for miRNA-21 sequence, experiments with 1MM sequence were carried out. At this time ssDNA/Au-Ni nanomotors were incubated with 1 nM 1-MM sequence for 15 min. The fluorescence intensities for the ssDNA/Au-Ni nanomotor (0 min), target miRNA-21, and 1-MM were given in **Figure 4**A. It was clearly seen from this figure that the ssDNA probe immobilized nanomotors were able to differentiate the target miRNA-21 and 1-MM effectively.

The optical microscopy images of Au-Ni nanomotors, ssDNA/Au-Ni nanomotors are shown in **Figure 4**B-a and b, respectively. Fluorescence responses of the ssDNA/Au-Ni nanomotors are clear (**Figure 4**B-b). After the incubation of these nanomotors with 0.05 nM (**Figure 4**B-c) and 0.1 nM (**Figure 4**B-d) target miRNA-21, there were small decreases in the fluorescence intensities as given quantitatively

above in **Figure 3**b. Optical images of the ssDNA/Au-Ni nanomotors after the hybridization protocol with 50 nM miRNA-21 (**Figure 4**B-e) and 100 nM miRNA-21 (**Figure 4**B-f) presented the fluorescence quenching better as expected.

The fluorescence intensity change of the hybridization of only ssDNA and miRNA-21 (without nanomotors) was also studied for 3 different miRNA-21 concentrations (**Figure S2**). Approximately 4-fold fluorescence changes were observed in the presence of nanomotors (**Figure 3**A). Thus, nanomotor based approach provided a sensitive sensing protocol compared to this control experiment.

3.3. Chemotherapeutic Drug Loading and Release with Au-Ni Nanomotors

Drug loading and release capabilities of Au-Ni nanomotors were examined using chemotherapeutic drug DOX. **Figure S3** schematically describes the physisorption loading of DOX onto Au-Ni nanomotors through hydrophobic interaction. For this Au-Ni nanomotors were initially modified with poly(sodium 4-styrenesulfonate) (PSS) as described in the experimental part. Subsequently, PSS/Au-Ni nanomotors were incubated with various amounts of chemotherapeutic agent (25 μM to 200 μM) prepared at pH 8.0 for 24 h. After this drug loading step, DOX/PSS/Au-Ni nanomotors were subjected to fluorescence intensity and speed measurements using optical microscopy. For the investigation of release profile of PSS/ Au-Ni nanomotors, they were put into pH 5.0 medium for 1 h and the fluorescence quenching on this pH-dependent nanomotors were checked. Besides fluorescence control, the speed changes were tracked. The polyelectrolyte layers generally have high loading ability and selectivity which makes them good candidates for drug delivery.[20] The conjugation between PSS and DOX includes not only electrostatic interaction between the negatively charged sulfonate group of the PSS and the amine group of the positively charged DOX, but also an additional hydrogen bond between the amino and hydroxyl groups of DOX and the sulfonate group of PSS.[18]

First, the effect of DOX concentration was investigated by probing the fluorescence intensities of PSS/Au-Ni nanomotors. The fluorescence intensity of the PSS/Au-Ni nanomotor under optical microscope was measured as 740 au The fluorescence intensity of 25 μM drug-loaded motor was measured as 1800 au; 2-fold fluorescence intensity was observed compared to the drug- unloaded motor. Fluorescence intensity of nanomotor loaded with 200 μM drug increased to 2150 au value (**Figure 5**A-green bars). An increase in fluorescence intensities of PSS/Au-Ni nanomotors were observed due to the increased amount of drug onto PSS/ Au-Ni nanomotors. As seen in **Figure 5**B, the speed of nanomotor decreased with increasing drug concentration (**Figure 5**B, purple bars). The drug-loaded nanomotors were then kept in phosphate buffer solution at pH 5.0 for drug releasing process and the same experimental procedure were repeated. **Figure 5**A (blue bars) shows the changes in fluorescence intensity of nanomotors for this condition. With a pH-dependent release, the flourescence intensity of 200 μM DOX-loaded nanomotors decreased about 48%, whereas it was about 7% for 25 μM DOX-loaded PSS/Au—Ni nanomotor. The decrease in the flourescence intensity of nanomotors with changing pH was related to the incerasing hyrophilicity of the DOX molecule in acidic medium. The amino group on the DOX molecule improved the water solubility and desorption capability at lower pH.12 The speed of nanomotors increased after the pH change due to the unloading of the drug from the nanomotor surface (**Figure 5**B, gray bars).

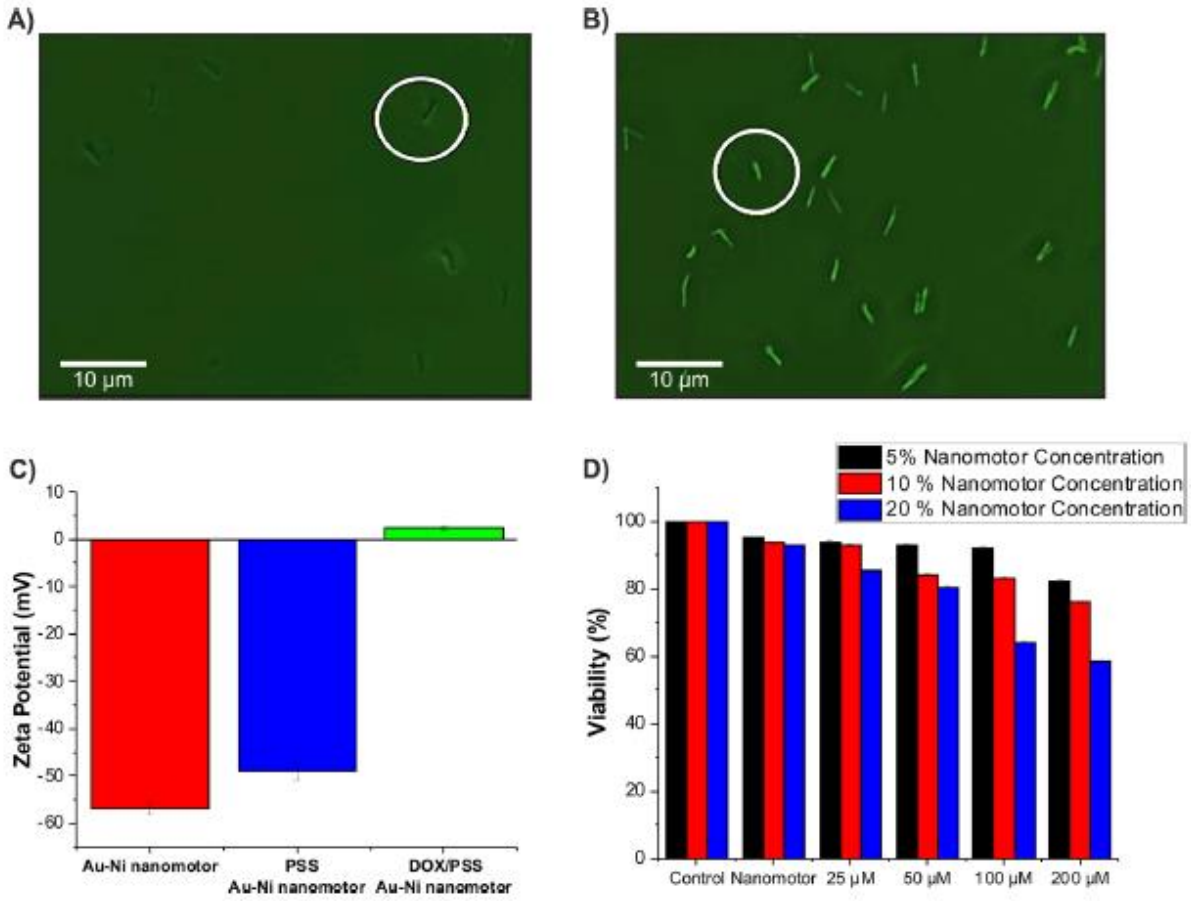

Figure 6. Fluorescence images of (A) PSS/Au—Ni nanomotors, (B) 200 μM-loaded DOX/PSS/Au—Ni nanomotors, (C) the zeta potentials of PSS/Au—Ni nanomotors and DOX/PSS/Au—Ni nanomotors (n = 3), (D) cytotoxicity assays and efficacy testing of the PSS/Au—Ni nanomotors as drug carriers: biocompatibility of nanomotors containing three different concentrations (5%, black; 10%, red; 20%, blue bars) and various concentrations of drug (25, 50, 100, 200 μM) (n = 3).

Video S3 shows the movements of 200 j«M DOX-loaded PSS/Au—Ni nanomotors before and after holding them at pH 5.0 media under applied magnetic field 22 mT.

Figure 6A,B illustrates changes in fluorescence intensity of PSS/Au—Ni nanomotors and DOX/PSS/Au—Ni nanomotors (for 200 µM of drug loading), respectively. After DOX loading, the fluorescence intensity of the nanomotor clearly increased. Zeta potential is an important factor to evaluate the storage stability of colloidal dispersion. The higher value of the zeta potential increases the particles' stability.[40,41] The zeta potential analysis shows that the Au—Ni nanomotors and PSS/Au—Ni nanomotors have a negative charge (—57 and —49.1 mV), whereas DOX/PSS/Au—Ni nanomotors have a positive charge (2.03 mV), as illustrated in **Figure 6**C. The positive zeta potential result of DOX/PSS/Au—Ni nanomotors presents the interaction between the negatively charged sulfonate group of the PSS and the positively charged amine group of DOX. Therefore, DOX adsorption is from the electrostatic interaction between the sulfonate groups of PSS and the amino groups of DOX. DOX/PSS/Au—Ni stored in the refrigerator is physically stable and does not flocculate under these conditions.

The data obtained and the **Video S3** revealed the possible use of PSS/Au—Ni nanomotors as drug carriers. In light of these promising results, biocompatibility and efficacy tests for the drug delivery vehicles were made using the primary mouse embryonic fibroblast cell. In order to determine the

toxicity profile of these nanomotors, the methylthiazolyldiphenyl-tetrazolium bromide (MTT) assay was chosen. MTT assay was performed to measure the cytotoxicity of DOX/PSS/Au— Ni nanomotors. Different amounts of DOX (25, 50, 100, and 200 μM) are loaded with various concentrations of nanomotors (5%, 10%, 20%) to see the effect of the nanomotor concentration on the cell viability. **Figure 6**D shows the MTT assay of the mouse embryonic fibroblast cell for 24 h exposure to DOX-loaded PSS/Au—Ni nanomotors. The nanomotors demonstrated biocompatibility (>80% viable cells) up to a concentration level of 50 µM DOX with 20% concentration of Au—Ni nanomotors (**Figure 6**D, blue) after the 24 h incubation period. Also, the concentration-dependent toxicity trend which was higher than nondrug loaded nanomotors was observed in all motor concentrations (>95% viable cells). DOX binds to DNA by intercalation and inhibits nucleic acid synthesis in the cell.[31] Therefore, the cell viability decreases with increasing drug concentration and nanomotor concen-tration.[38] When biocompatibilities of nanomotors are examined, no obvious cytotoxicity was detected until 100 μM DOX (20% nanomotor concentration). Furthermore, it was the same for 200 μM DOX at 10% and 20% of nanomotor concentrations.

Table 1. Comparison of Nanomaterial-Based MTT Assay—Viability Studies

nano/micromotors	DOX/carrier concentration	treatment time	cell viability	reference
reduced nanographene oxide/Pt	3 mg mL^{-1}/3 mg mL^{-1}	24 h	<30%	42
magnetic silica composite	28 μM/30 μg mL^{-1}	24 h	<40%	43
silica spheres	1.0 mM/0.5 mg mL^{-1}	24 h	<70%	17
Au–Ni	200 μM/0.05 mg mL^{-1} and 0.1 mg mL^{-1}	24 h	<80%	this study

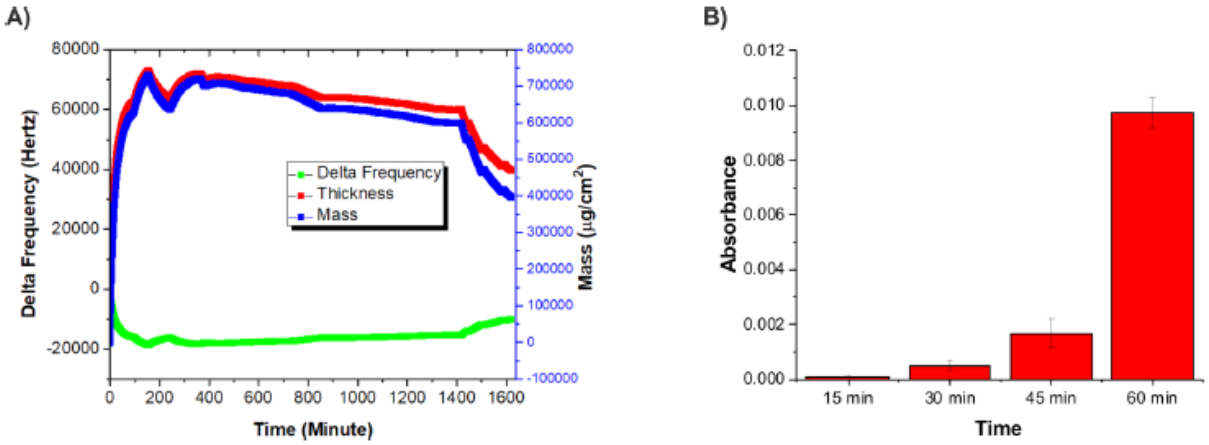

Figure 7. (A) QCM measurements of the PSS/Au-Ni nanomotors for loading and release of DOX and (B) UV-vis absorbance spectra of the released DOX from QCM electrode (n = 3).

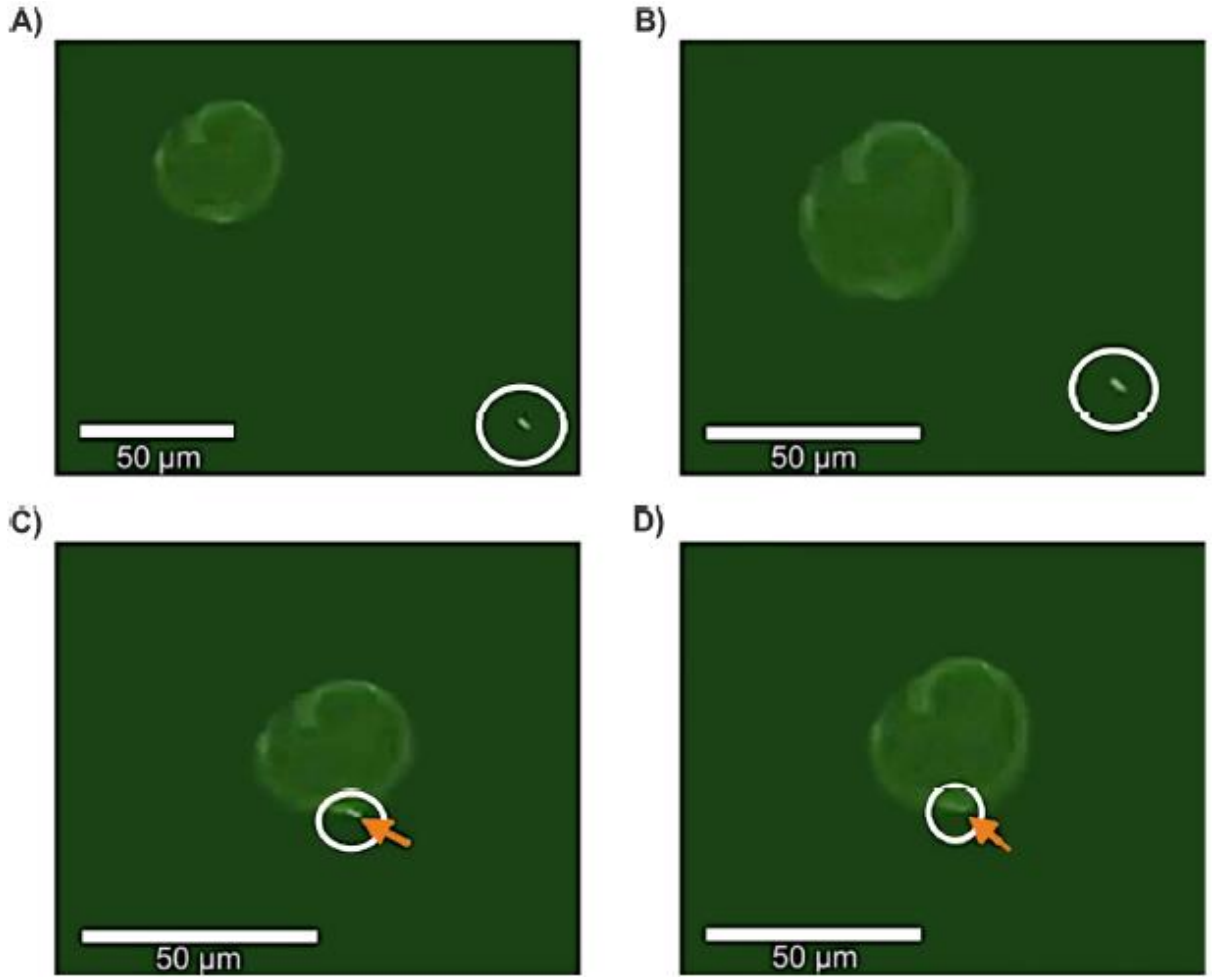

Figure 8. Movement of the ssDNA/Au-Ni nanomotor toward the MCF-7 cell under a 22 mT magnetic field: (A) movement, (B) approaching, (C) penetrating, and (D) inside the MCF-7 cell.

Especially, 200 μM DOX-loaded nanomotors with concentration of 20% showed cytotoxic effect for mouse embryonic fibroblast cells with a viability decreased down to 60%. The nanomotors presented in this study highlighted possible targeted drug delivery and thus cancer treatment with them.

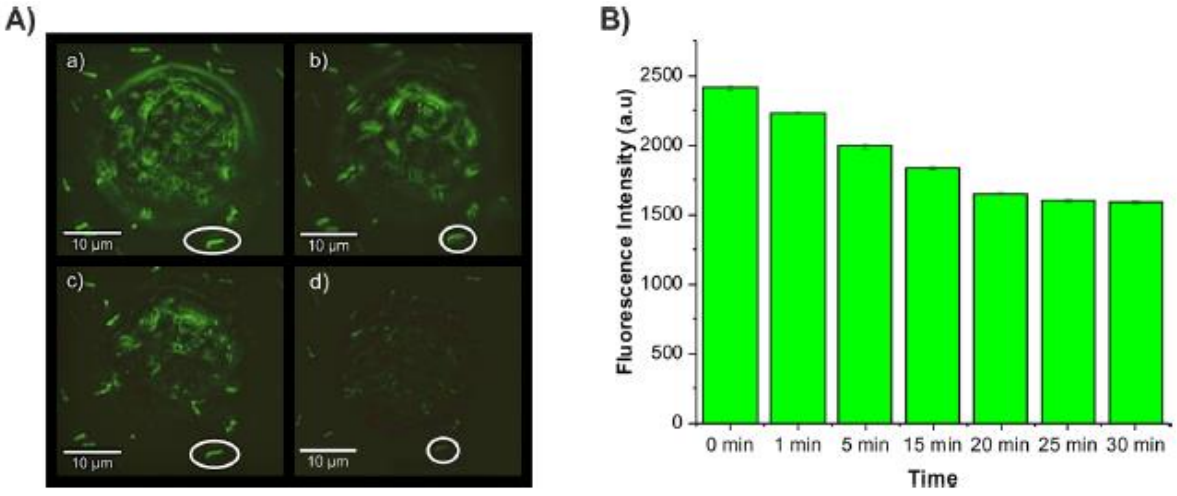

Figure 9. (A) Co-incubated DOX-loaded Au-Ni nanomotors and MCF-7 cells: NIR exposure for (a) 1 min, (b) 5 min, (c) 15 min, and (d) 20 min; (B) effect of NIR laser application time on fluorescence intensities of drug-loaded motors (n = 3).

In addition, reduced side effects of the given drug provided benefits for the development of advanced drug delivery systems.[23] Comparison between previous studies and DOX/PSS/Au-Ni nanomotors are very promising and comparable. They had lower toxicity compared to the literature (**Table 1**).

Moreover, QCM measurements were examined to confirm the loading and release process of DOX onto/from PSS/Au-Ni nanomotors. For this purpose, PSS/Au-Ni nanomotors were dispersed in ethanol and dried on a QCM gold electrode and placed in the cell. A 200 μM DOX solution prepared in pH 8.0 phosphate buffer was injected during 24 h (1440 min). **Figure 7**A shows the changes in mass increase and frequency decrease on the electrode after starting the injection of the drug onto the QCM electrode. At about 8 h (480 min), the drug loading capacity of the nanomotors leveled off. Thus, the mass of the electrode remained almost constant. At the end of 24 h, pH 5.0 phosphate buffer was injected to DOX-loaded nanomotors on the electrode. In this case, the mass of the electrode started to decrease sharply because of the released drug from the nanomotors. When the loading and release processes were compared, it was observed that the release process (160 min) was faster than the loading process (1440 min). It was also indicated by Xing et al. that at pH 5.0, which is known as the endosomal pH of cancer cells, DOX released significantly faster.[44] During the release process in QCM analysis, the released solutions were subjected to UV-vis spectroscopy measurements every 15 min. The characteristic absorption band of DOX is around 480 nm.[40] **Figure 7**B shows the absorbance values of the released drug solutions from Au-Ni nanomotors at 480 nm. These results were in a good correlation with the QCM results. With increasing time, the UV-vis absorption band intensity increased. Furthermore, **Figure S4** illustrates the absorbance spectra of the DOX solution (black), DOX/PSS/Au—Ni nanomotor solution after several washing steps with pH 8.0 buffer (red), and after 60 min incubation in pH 5.0 buffer (blue).

3.4. In Vitro Applications of Au-Ni Nanomotors

At last, in vitro applications of the Au-Ni nanomotors were performed to recognize miRNA-21, carry drugs, and penetrate MCF-7 breast cancer cells under magnetic control. For the recognition of the target miRNA-21 expression of intact cancer cells, ssDNA/Au-Ni nanomotors were directed to a breast cancer cell line. It was observed that the ssDNA/Au-Ni nanomotors moved in the cell medium and penetrated MCF-7 breast cancer cells successfully under magnetic control.

Figure 8 and **Video S4** show the guided movement of the nanomotors toward the MCF-7 cell under a 22 mT magnetic field. The movement of ssDNA/Au-Ni nanomotors was changed from its original straight line by a magnet. However, nanomotors continued their path without external interference and arrived at the cell membrane. The nanomotor approaches the cell under the magnetic field and penetrates the MCF-7 cell (**Figure 8**A-C). After it attaches to the cell, the fluorescence intensity decreased from 2600 to 2000 au at about 2 min due to the overexpressed miRNA-21 in the MCF-7 cell (**Figure 8**D).

Afterward, the drug delivery application was demonstrated. **Video S5** presents the movement of a single 200 μM DOX-loaded PSS/Au-Ni nanomotor at its straight line under a magnetic field and penetrating a cancer cell. The drug release studies were then carried out using a NIR triggered approach.[22] NIR laser (800 nm) was applied to drug-loaded nanomotors until 30 min while they were held at close proximity to the cells. Optical microscopy images of MFC-7 cells and nanomotors during 1, 5, 15, and 20 min of NIR applications are shown in **Figure 9**A. **Figure 9**B shows the fluorescence intensity changes of a motor during NIR laser application. After 20 min, the fluorescence intensity of the nanomotor remained almost constant. The release profile of the motors under NIR are also given in **Figure S5**. The magnetic directionality of the motor presented its successfully controlled and guided

motion under an applied external magnetic field. This facile movement and surface functionality of the nanomotors provided outstanding biomedical applications.

In this study, the sensitive detection of an important cancer biomarker miRNA-21 and pH dependent/near-infrared (NIR) triggered release of a commonly used chemotherapeutic drug doxorubicin (DOX) were targeted. Thus, corresponding experiments were not affected by the fluorescence intensity of the nanomotors. However, nanomotor applications where the nanomotor uptake was crucial and targeted,[35,45] it was known that the number of cells definitely affected the fluorescence intensity of the nanomotors.

4. CONCLUSIONS

The fabrication and use of Au-Ni magnetic nanowires as nanomotors for a clinically relevant biomarker miRNA-21 detection and controlled anticancer drug delivery were described in the present work. The nanomotors were fabricated with the electrochemical preparation of Au nanowires followed by the DC magnetron sputtering of the Ni part. To the best of our knowledge, DC magnetron sputtering-based preparation has never been used for this purpose. This method served homogeneous distribution and also rapid deposition of the metal directly. One of the most important advantages of these novel nanomotors was its fuel-free magnetic propulsion. The fabricated Au-Ni nanomotors also had a significant improvement at their speeds. Sensitive and selective miRNA-21 detection was achieved using ssDNA/Au-Ni nanomotors with low detection limits of 2.9 and 1.6 pM for fluorescence and speed-based detection, respectively. Magnetically powered DOX/PSS/Au-Ni nanomotors presented good pH-dependent drug release. In addition, the DOX/PSS/Au-Ni nanomotors guided on MCF-7 cells exhibited efficient and controlled delivery of the drug. Toxicity/biocompability of the nanomotors that were tested with MTT assays were found to be very promising. In vitro applications for the ssDNA/Au-Ni and DOX/PSS/Au-Ni nanomotors were successfully performed. In conclusion, the Au-Ni-based novel nanomotors developed in this study are expected to be useful for important future bioapplications in various media such as cell medium, serum, and urine.

REFERENCES

(1) Yuan, K.; De La Asunción-Nadal, V.; Jurado-Sánchez, B.; Escarpa, A. 2D Nanomaterials Wrapped Janus Micromotors with Built-in Multiengines for Bubble, Magnetic, and Light Driven Propulsion. Chem. Mater. 2020, 32 (5), 1983-1992.

(2) Liu, M.; Wang, Y.; Kuai, Y.; Cong, J.; Xu, Y.; Piao, H. G.; Pan, L.; Liu, Y. Magnetically Powered Shape-Transformable Liquid Metal Micromotors. Small 2019, 15 (52), 1905446.

(3) Katuri, J.; Ma, X.; Stanton, M. M.; Sánchez, S. Designing Micro-and Nanoswimmers for Specific Applications. Acc. Chem. Res. 2017, 50 (1), 2-11.

(4) Wang, H.; Pumera, M. Fabrication of Micro/Nanoscale Motors. Chem. Rev. 2015, 115 (16), 8704- 8735.

(5) Xu, D.; Wang, Y.; Liang, C.; You, Y.; Sanchez, S.; Ma, X. Self-Propelled Micro/Nanomotors for Biomedical Cargo Transportation. Small 2020, 16 (27), 1902464.

(6) Medina-Sánchez, M.; Xu, H.; Schmidt, O. G. Micro- and NanoMotors: The New Generation of ug Carriers. Ther. Delivery 2018, 9 (4), 303-316.

(7) Xu, T.; Xu, L. P.; Zhang, X. Ultrasound Propulsion of Micro-/ Nanomotors. Appl. Mater. Today 2017, 9, 493-503.

(8) Li, J.; Li, T.; Xu, T.; Kiristi, M.; Liu, W.; Wu, Z.; Wang, J. Magneto-Acoustic Hybrid Nanomotor. Nano Lett. 2015, 15 (7), 4814-4821.

(9) Liu, M.; Pan, L.; Piao, H.; Sun, H.; Huang, X.; Peng, C.; Liu, Y. Magnetically Actuated Wormlike Nanomotors for Controlled Cargo Release. ACS Appl. Mater. Interfaces 2015, 7 (47), 26017-26021.

(10) Wang, C.; Dong, R.; Wang, Q.; Zhang, C.; She, X.; Wang, J.; Cai, Y. One Modification, Two Functions: Single Ni-Modified Light-Driven ZnO Microrockets with Both Efficient Propulsion and Steerable Motion. Chem. - Asian J. 2019, 14, 2485-2490.

(11) Li, J.; de Avila, B. E.-F.; Gao, W.; Zhang, L.; Wang, J. Micro/ Nanorobots for Biomedicine: Delivery, Surgery, Sensing, and Detoxification Sci. Robot.2017, 2, eaam6431.

(12) Esteban-Fernández De Avila, B.; Martín, A.; Soto, F.; Lopez-Ramirez, M. A.; Campuzano, S.; Vásquez-Machado, G. M.; Gao, W.; Zhang, L.; Wang, J. Single Cell Real-Time MiRNAs Sensing Based on Nanomotors. ACS Nano 2015, 9 (7), 6756-6764.

(13) Qiu, F.; Fujita, S.; Mhanna, R.; Zhang, L.; Simona, B. R.; Nelson, B. J. Magnetic Helical Microswimmers Functionalized with Lipoplexes for Targeted Gene Delivery. Adv. Funct. Mater. 2015, 25 (11), 1666-1671.

(14) Esteban-Fernández De Avila, B.; Ramírez-Herrera, D. E.; Campuzano, S.; Angsantikul, P.; Zhang, L.; Wang, J. Nanomotor-Enabled PH-Responsive Intracellular Delivery of Caspase-3: Toward Rapid Cell Apoptosis. ACS Nano 2017, 11 (6), 5367-5374.

(15) Beltrán-Gastélum, M.; Esteban-Fernández de Avila, B.; Gong, H.; Venugopalan, P. L.; Hianik, T.; Wang, J.; Subjakova, V. Rapid Detection of AIB1 in Breast Cancer Cells Based on Aptamer-Functionalized Nanomotors. ChemPhysChem 2019, 20, 3177-3180.

(16) Kagan, D.; Laocharoensuk, R.; Zimmerman, M.; Clawson, C.; Balasubramanian, S.; Kang, D.; Bishop, D.; Sattayasamitsathit, S.; Zhang, L.; Wang, J. Rapid Delivery of Drug Carriers Propelled and Navigated by Catalytic Nanoshuttles. Small 2010, 6 (23), 27412747.

(17) Hortelao, A. C.; Patino, T.; Perez-Jiménez, A.; Blanco, A.; Sánchez, S. Enzyme-Powered Nanobots Enhance Anticancer Drug Delivery. Adv. Funct. Mater. 2018, 28 (25), 1705086.

(18) Garcia-Gradilla, V.; Sattayasamitsathit, S.; Soto, F.; Kuralay, F.; Yardimci, C.; Wiitala, D.; Galarnyk, M.; Wang, J. Ultrasound-Propelled Nanoporous Gold Wire for Efficient Drug Loading and Release. Small 2014, 10 (20), 4154-4159.

(19) Chen, W.; Sun, M.; Fan, X.; Xie, H. Magnetic/PH-Sensitive Double-Layer Microrobots for Drug Delivery and Sustained Release. Appl. Mater. Today 2020, 19, 100583.

(20) Wu, Y.; Lin, X.; Wu, Z.; Mohwald, H.; He, Q. Self-Propelled Polymer Multilayer Janus Capsules for Effective Drug Delivery and Light-Triggered Release. ACS Appl. Mater. Interfaces 2014, 6 (13), 10476-10481.

(21) Singh, V. V.; Kaufmann, K.; de Avila, B. E. F.; Karshalev, E.; Wang, J. Molybdenum Disulfide-Based Tubular Microengines: Toward Biomedical Applications. Adv. Funct. Mater. 2016, 26 (34), 6270-6278.

(22) Garcia-Gradilla, V.; Orozco, J.; Sattayasamitsathit, S.; Soto, F.; Kuralay, F.; Pourazary, A.; Katzenberg, A.; Gao, W.; Shen, Y.; Wang, J. Functionalized Ultrasound-Propelled Magnetically Guided Nanomotors: Toward Practical Biomedical Applications. ACS Nano 2013, 7 (10), 9232-9240.

(23) Jiao, X.; Wang, Z.; Xiu, J.; Dai, W.; Zhao, L.; Xu, T.; Du, X.; Wen, Y.; Zhang, X. NIR Powered Janus Nanocarrier for Deep Tumor Penetration. Appl. Mater. Today 2020, 18, 100504.

(24) Gao, W.; Kagan, D.; Pak, O. S.; Clawson, C.; Campuzano, S.; Chuluun-Erdene, E.; Shipton, E.; Fullerton, E. E.; Zhang, L.; Lauga, E.; Wang, J. Cargo-Towing Fuel-Free Magnetic Nanoswimmers for Targeted Drug Delivery. Small 2012, 8 (3), 460-467.

(25) Gao, W.; Sattayasamitsathit, S.; Manesh, K. M.; Weihs, D.; Wang, J. Magnetically Powered Flexible Metal Nanowire Motors. J. Am. Chem. Soc. 2010, 132 (41), 14403-14405.

(26) Wang, Q.-l.; Wang, C.; Dong, R.-f.; Pang, Q.-q.; Cai, Y.-p. Steerable Light-Driven TiO2-Fe Janus Micromotor. Inorg. Chem. Commun. 2018, 91, 1-4.

(27) Wu, F.; Yang, D.; Huang, X.; Yi, L.; Liu, M.; Pan, L. Ultrafast Bubble-Propelled and Magnetic-Field-Navigated Porous Catalytic Janus Micromotor. J. Nanosci. Nanotechnol. 2019, 19 (7), 4154-4159.

(28) Bahreyni, A.; Rezaei, M.; Bahrami, A.; Khazaei, M.; Fiuji, H.; Ryzhikov, M.; Ferns, G. A.; Avan, A.; Hassanian, S. M. and Therapeutic Potency of MicroRNA 21 in the Pathogenesis of Colon Cancer, Current Status and Prospective. J. Cell. Physiol. 2019, 234 (6), 8075-8081.

(29) Gao, W.; de Avila, B. E. F.; Zhang, L.; Wang, J. Targeting and Isolation of Cancer Cells Using Micro/Nanomotors. Adv. Drug Delivery Rev. 2018, 125, 94-101.

(30) Kwak, M.; Jung, I.; Kang, Y. G.; Lee, D. K.; Park, S. Multi-Block Magnetic Nanorods for Controlled Drug Release Modulated by Fourier Transform Surface Plasmon Resonance. Nanoscale 2018, 10 (39), 18690-18695.

(31) Chen, R.; Sun, P.; Chu, X.; Pu, X.; Yang, Y.; Zhang, N.; Zhao, Y. Synergistic Treatment of Tumor by Targeted Biotherapy and Chemotherapy via Site-Specific Anchoring of Aptamers on Dna Nanotubes. Int. J. Nanomed. 2020, 15, 1309-1320.

(32) 2. Fluorescence-Based Assays for Measuring Doxorubicin in Biological Systems. Physiol. Behav. 2019, 176 (3), 139-148.

(33) Cogal, G. C.; Das, P. K.; Li, S.; Oksuz, A. U.; Bhethanabotla, V. R. Unraveling the Autonomous Motion of Polymer-Based Catalytic Micromotors Under Chemical A Acoustic Hybrid Power. Adv. NanoBio Res.2021, 1 (2), 2000009.

(34) Sandstrom, P.; Boncheva, M.; Akerman, B. Nonspecific and Thiol-Specific Binding of DNA to Gold Nanoparticles. Langmuir 2003, 19 (18), 7537-7543.

(35) Wan, M.; Chen, H.; Wang, Q.; Niu, Q.; Xu, P.; Yu, Y.; Zhu, T.; Mao, C.; Shen, J. Bio-Inspired Nitric-Oxide-Driven Nanomotor. Nat. Commun. 2019, 10 (1) DOI: 10.1038/s41467-019-08670-8.

(36) Burdick, J.; Laocharoensuk, R.; Wheat, P. M.; Posner, J. D.; Wang, J. Synthetic Nanomotors in Microchannel Networks: Directional Microchip Motion and Controlled Manipulation of Cargo. J. Am. Chem. Soc. 2008, 130 (26), 8164-8165.

(37) Ahmed, S.; Wang, W.; Mair, L. O.; Fraleigh, R. D.; Li, S.; Castro, L. A.; Hoyos, M.; Huang, T. J.; Mallouk, T. E. Steering Acoustically Propelled Nanowire Motors toward Cells in a Biologically Compatible Environment Using Magnetic Fields. Langmuir 2013, 29 (52), 16113-16118.

(38) Cheng, Y.; Dong, L.; Zhang, J.; Zhao, Y.; Li, Z. Recent Advances in MicroRNA Detection. Analyst 2018, 143 (8), 17581774.

(39) Oksuz, L.; Yurdabak Karaca, G.; Kuralay, F.; Uygun, E.; Koc, I. U.; Uygun Oksuz, A. Preparation of Self-Propelled Cu-Pt Micromotors and Their Application in MiRNA Monitoring. Turk. J. Chem. 2018, 42 (6), 1744-1754.

(40) Palai, P. K.; Mondal, A.; Chakraborti, C. K.; Banerjee, I.; Pal, K.; Rathnam, V. S. S. Doxorubicin Loaded Green Synthesized Nanoceria Decorated Functionalized Graphene Nanocomposite for Cancer-Specific Drug Release. J. Cluster Sci 2019, 30 (6), 15651582.

(41) Zhou, M.; Hou, T.; Li, J.; Yu, S.; Xu, Z.; Yin, M.; Wang, J.; Wang, X. Self-Propelled and Targeted Drug Delivery of Poly(Aspartic Acid)/Iron-Zinc Microrocket in the Stomach. ACS Nano 2019, 13 (2), 1324-1332.

(42) Khezri, B.; Beladi Mousavi, S. M.; Krejcová, L.; Heger, Z.; Sofer, Z.; Pumera, M. Ultrafast Electrochemical Trigger Drug Delivery Mechanism for Nanographene Micromachines. Adv. Funct. Mater. 2019, 29 (4), 1806696.

(43) Zhou, Y.; Zeng, Y.; Huang, S.; Xie, Q.; Fu, Y.; Tan, L.; Ma, M.; Yao, S. Quartz Crystal Microbalance Monitoring of Intervention of Doxorubicin-Loaded Core-Shell Magnetic Silica Nanospheres on Human Breast Cancer Cells (MCF-7). Sens. Actuatorsý B 2012, 173, 433-440.

(44) Zhou, T.; Zhou, X.; Xing, D. Controlled Release of Doxorubicin from Graphene Oxide Based Charge-Reversal Nanocarrier. Biomaterials 2014, 35 (13), 4185-4194.

(45) Sun, J.; Mathesh, M.; Li, W.; Wilson, D. A. Enzyme-Powered Nanomotors with Controlled Size for Biomedical Applications. ACS Nano 2019, 13 (9), 10191-10200.